Asymmetric Cooperation Control of Dual-Arm Exoskeletons Using Human Collaborative Manipulation Models

Zhijun Li, *Senior Member, IEEE*, Guoxin Li, Xiaoyu Wu, Zhen Kan, *Member, IEEE*, Hang Su, *Member, IEEE*, and Yueyue Liu

***Abstract*—The exoskeleton is mainly used by subjects who suffer muscle injury to enhance motor ability in the daily life environment. Previous research seldom considers extending human collaboration skills to human–robot collaborations. In this article, two models, that is: 1) the *following the better* model and 2) the *interpersonal goal integration* model, are designed to facilitate the human–human collaborative manipulation in tracking a moving target. Integrated with dual-arm exoskeletons, these two models can enable the robot to successfully perform target tracking with two human partners. Specifically, the manipulation workspace of the human–exoskeleton system is divided into a human region and a robot region. In the human region, the human acts as the leader during cooperation, while, in the robot region, the robot takes the leading role. A novel region-based Barrier Lyapunov function (BLF) is then designed to handle the change of leader roles between the human and the robot and ensures the operation within the constrained human and robot regions when driving the dual-arm exoskeleton to track the moving target. The designed adaptive controller ensures the convergence of tracking errors in the presence of region switches. Experiments are performed on the dual-arm robotic exoskeleton for the subject with muscle damage or some degree of motor dysfunctions to evaluate the proposed controller in tracking a moving target, and the experimental results demonstrate the effectiveness of the developed control.**

***Index Terms*—Asymmetric cooperation manipulation, dual-arm exoskeletons, human–human cooperation, region-based Barrier Lyapunov function (BLF).**

Manuscript received 7 August 2020; revised 23 December 2020 and 15 March 2021; accepted 14 September 2021. Date of publication 12 October 2021; date of current version 17 October 2022. This work was supported in part by the National Natural Science Foundation of China under Grant 62133013 and Grant U1913601; in part by the Anhui Provincial Natural Science Foundation, Anhui Energy-Internet Joint Program under Grant 2008085UD01; in part by the Major Science and Technology Projects of Anhui Province under Grant 202103a05020004; and in part by the National Key Research and Development Program of China under Grant 2018AAA0102900, Grant 2020YFC2007900, and Grant 2018YFC2001602. This article was recommended by Associate Editor J. Q. Gan. *(Corresponding author: Zhijun Li.)*

This work involved human subjects or animals in its research. Approval of all ethical and experimental procedures and protocols was granted by Ethics Committee of Yueyang Integrated Traditional Chinese and Western Medicine Hospital Affiliated with Shanghai University of Traditional Chinese Medicine under Application No. 2019-014.

Zhijun Li, Guoxin Li, and Zhen Kan are with the Department of Automation, University of Science and Technology of China, Hefei 230026, China, and also with the Institute of Artificial Intelligence, Hefei Comprehensive National Science Center, Hefei 230031, China (e-mail: zjli@ieee.org).

Xiaoyu Wu was with the Department of Automation, University of Science and Technology of China, Hefei 230026, China. He is now with the Department of Biomedical Engineering, the National University of Singapore, Singapore.

Hang Su is with the Dipartimento di Elettronica, Informazione e Bioingegneria, Politecnico di Milano, 20133 Milan, Italy (e-mail: hang.su@polimi.it).

Yueyue Liu is with the College of Automation, South China University of Technology, Guangzhou 510640, China (e-mail: lyy8313167@163.com).

Color versions of one or more figures in this article are available at https://doi.org/10.1109/TCYB.2021.3113709.

Digital Object Identifier 10.1109/TCYB.2021.3113709

I. Introduction

CURRENTLY, stroke and various diseases cause limb movement disorders, which is becoming a leading cause of adult disability [1]. High-intensity and task-specific upper limb treatment consists of active and highly repetitive movements, which is considered to be one of the most effective approaches to arm and hand function restoration [2]. However, traditional methods from therapists are far from being able to complete such rehabilitation training, which, in turn, affects motor task performance, even further leading to the impaired arm motor function. Robot exoskeletons-supported training is emerging as a solution to aid the subjects who suffer muscle injury by providing high-intensity, repetitive, and task-specific treatment to enhance motor ability in the daily life environment, which has become a research hotspot.

Recently, robotic power-assist exoskeletons have been successfully developed for human power augmentation, rehabilitation training, etc. [3]–[5]. Due to the structural resemblance to human arms, dual-arm exoskeletons are considered a powerful tool to enhance human capabilities in dealing with challenging tasks, for example, lifting heavy objects. As the exoskeleton interacts and cooperates closely with humans, much research has been proposed for the human–robot interactions [14]–[16], [18], [28]. In [14], the interaction force is used to help the exoskeleton robot understand the motion intention of the human operator to realize cooperative manipulation under the assumption that the force is equal to the force exerted by the subject and can be obtained by the force sensor. In [16], the motion-coupled control and force-coupled control are investigated to improve the motor ability of humans. In [28], an optimization approach for reshaping the physical interactive trajectory is presented in the co-manipulation tasks. In [15], a human-inspired control with force and impedance adaptation is proposed to interact with unknown environments and exhibit this biological behavior. In [18], an approach of coordination control of a dual-arm exoskeleton robot is developed based on human impedance

TABLE I
NOMENCALATURE

T	The collection of position, velocity and acceleration of moving target in a task
t	The position of moving target in a task
$\mathbb{R}$	The set
u	The control input in a task
X_h	The collection of position, velocity and acceleration of the human hand in a task
x_h	The position of the human hand in a task
K_p	The control gain for position
K_v	The control gain for velocity
K_a	The control gain for accelaration
K	The collection of the control gain
A, B	The coefficient of time derivation of T
m	The point-mass in the model
f_e	The interaction force between human and exoskeleton or the haptic force or measurable by force sensor
E	The collection of the error
e	The error for position
e_m	The tracking error of the master
e_f	The tracking error of the follower
x_m	The position of the master
x_f	The position of the follower
M_e	The diagonal matrices of the mass
B_e	The diagonal matrices of the damper
K_e	The diagonal matrices of the stiffness
$\hat{t}$	The estimated position of the target
$M_i(q_i), M_{xi}$	The inertia matrix
$i = m, f$	m represents the master, f represents the follower
$C_i(q_i), C_{xi}$	The centrifugal and Coriolis torques
$G_i(q_i), G_{xi}$	The vector of gravitational torque
τ_i	The vector of control input
τ_{ei}	The torque exerted by human
x_i	The positions of robotic exoskeletons end-effector in Cartesian space
q_i	The joint variable of the exoskeleton robot
$h_i(\cdot)$	A nonlinear transformation function
$J_i(q)_i, J_i$	The Jacobian matrix from joint space to Cartesian space
f_i	The control input force
f_{ei}	The external force exerted by human
φ_1, φ_2	$n-$ dimensional vector
θ	Constant parameters vector
$\phi(\varphi_1, \varphi_2, x_i, \dot{x}_i)$	A regressor function
z_i	The error for position
x_{ri}	The reference position in task space
r_i	The radius of the human region
$f(z_i)$	The function for human region
$P(z_i)$	The function for potential energy
K_i	The constant
N	The order of the function
k_{ci}, k_{di}	The positive constants
V_1	The Barrier Lyapunov Function
α_i	The stabilizing function
β	A positive constant
$Y_{di}(x_i, \dot{x}_i, \alpha_i, \dot{\alpha}_i)$	A regressor function
$\hat{\theta}_{di}$	The estimate of θ_{di}
$\hat{M}_{xi}, \hat{C}_{xi}, \hat{G}_{xi}$	The approximate model for M_{xi}, C_{xi}, G_{xi}
γ_{di}	The control gain of adaptation
$\triangle\theta_{di}$	The difference for θ_{di} and $\hat{\theta}_{di}$
g_i, w, K_{si}	The term and coefficient of control law
W_i	A non-negative variable
ς	The integral variable
$\lambda_{min}(K_{si})$	The minimum eigenvalue
$L_2[e]$	The average tracking error
T_f	The total running time
$L_2[\tau]$	The average control input
l_1, l_2	The length of two links
F_{xi}, F_{yi}	The interaction force of group i

transfer skills, where the human stiffness and position profiles are transferred to the slave robot arm. In addition, human–robot physical coordination can be found in many applications,

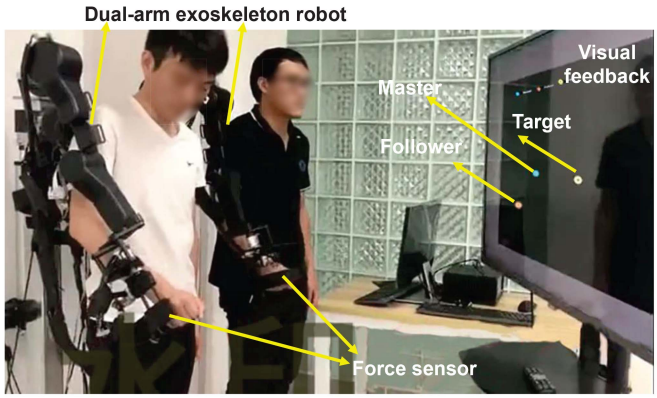

Fig. 1. Developed dual-arm exoskeleton robot and the experimental configuration. In the experiment, two partners manipulate their own robotic exoskeleton to track a randomly moving yellow target cursor based on visual feedback from the screen, and the blue cursor and red cursor represent the position of the master end effector and follower end effector, respectively.

for example, in [7]–[10]. The human–robot interaction task can be either discrete [8] or continuous [9], where a direct coupling of dyads can be realized by stiff devices, such as a crank [11], or by robotic devices [12]. There are several metrics used in previous studies, such as the energy exchange of partners [8], superior measures [8], target distance [13], and interaction force [9] for quantitative analysis. In [21], a model that computes the interaction force during a dyadic cooperative object manipulation task was presented. The model was used in a control strategy to enable robots to collaborate with humans. In [22], a robotic-assistive approach using the human–robot interface was presented for the bilateral movement training under the consideration of the principles of plasticity, and objective assessment tools to monitor the change.

However, few existing results in the literature consider extending human collaboration skills to human–robot collaboration. We considered such an extension through the dual-arm exoskeleton experiment platform shown in Fig.1, where two partners manipulate their own robotic exoskeletons to track a randomly moving red target based on visual feedback from the screen, where the cursor represents the position of the end effector. However, the cooperation between the dual-arm exoskeletons and the two human partners is rather challenging. For instance, it remains largely unknown how the two partners with physical interaction can effectively coordinate in a continuous tracking task and how two human partners with exoskeletons can successfully cooperate and coordinate in various missions. Therefore, it is necessary to develop a cooperative control strategy that can enable successful interaction and coordination between the dual-arm exoskeleton and the two partners in performing desired tracking missions.

Bimanual tasks depend upon the cooperation and coordination between the human's arms. Especially, asymmetrical bimanual manipulation is a common task for humans. Indeed, bimanual tasks depend upon the cooperation and coordination between the human's arms. Two arms coordinate while being in physical contact and fulfilling complementary aspects of the task: one arm is mostly assistive while the other performs active manipulation. Such a task can be executed either autonomously by a bimanual robot, or collaboratively by a

single robotic arm performing the assistive or active role in collaboration with a human, for example, it is extremely inconvenient to cut a fruit with only one hand, but it becomes easier with the other hand holding it [32]. Therefore, asymmetric cooperation control provides the users with the ability to individually control each robot end effector's motion, to successfully execute asymmetric bimanual tasks. One issue here is that, while the individual coordination of the robot end effectors is necessary for executing certain complex tasks, these works mainly emphasize the autonomy of robots, and few works consider the role of humans in the operation process. As for dual-arm exoskeletons, cooperation control of humans and exoskeletons must be considered to ensure the control compliance and the safety of humans. Moreover, the most important issue is the problem of extending human collaboration skills to human–robot collaborations, which has great significance in the treatment of exoskeleton rehabilitation.

Therefore, it is necessary to study the problem of asymmetric cooperation control. Human–human collaboration and various models for human interaction have been extensively studied in [6], [14], and [19]. However, due to the physical nature of the task, it is inherently vague how the interaction force can be recovered from the force exerted by humans. To address this ambiguity, various models for the interaction force have been proposed. For example, in [6], a continuous tracking task has been shown to achieve the coordination between two partners mediated by switching information on the current motion goal through haptics, that is, the sensory modality related to tactile and proprioceptive senses. In [14], in order to make the robot flexible and adaptable, a novel human cooperation strategy is proposed by using two upper limbs of the exoskeleton robot. In [19], by using the visual-motion rotation adaptation paradigm, the adaptability of arm motion to both static and moving targets was studied (i.e., pursuit or tracking). Contu *et al.* [23] have demonstrated the role of combining the haptic and visual feedback in a coupled bimanual task, and the task is driven by the dominant and nondominant hands. It has been shown that the task performance of manipulating the object would be degraded without tactile feedback. In [24], a remote task was studied, which involves controlling a single heavy object through two asymmetrical slaves: 1) a joystick and 2) an arm. The results show that the two cooperators can be more efficient in performing the maneuvering and mounting task than either bimanual or single operators. In general, a better understanding of human bimanual coordination while interacting with the robot may lead to improved control and performance in a variety of contexts.

Previous works [42]–[44] have been researched by the use of learning methods from humans. In [32], a parametrization of asymmetrical bimanual tasks is extracted from human demonstration. In [33], a framework that combines the benefits of kinesthetic teaching and attentional supervision was proposed to allow natural teaching by demonstration and flexible/collaborative execution of structured tasks. In [34], a novel approach for intuitive and natural physical human–robot interaction in cooperative tasks was proposed, where robot behavior naturally evolves into a cooperative task through initial learning by demonstration. In this case, the desired movement is predefined based on either the precise environmental knowledge [29], [30] or the use of complex motion that learning combined learning the task model and learning feedforward control [25]. Nevertheless, solving all problems by solely relying on learning is not a viable solution as learning requires data for training and, in most cases, this process is tedious.

In addition, these studies did not consider various physical constraints that exist in robotic systems, such as safety specifications and physical limits. To address the control safety in the process of human–robot interaction, some researchers adopted a framework of a hard switching of multiple controllers (e.g., a proxy-based controller plus a torque controller [35]). However, the hard switching may result in an overall discontinuous control input, which further causes the chattering movement of a robot or even compromises the safety of humans. In [36], an adaption method was proposed for human–robot collaboration to adjust the robot's role to lead or follow the human. In [37], a physically interactive trajectory deformations algorithm based on impedance control was presented which allowed the human to modulate both the actual and desired trajectories of the robot. In [25], impedance control was presented for the human–robot cooperative task, where the robot predicts and adapts to the human motion. The expected performance of the robot system is designated as the expected impedance describing the relationship between the desired motion of the robot and the external force imposed by the human operator. However, most human–robot interaction control schemes commonly assume the robot dynamics to be exactly known or do not take it into account. Since the system can exhibit drift in position errors in performing tracking tasks, the generated torque can potentially cause damages to the users.

Many advanced control algorithms have been proposed to address the uncertainty of robot dynamics and disturbance. In [38], a direct adaptive robust tracking control with a projection-type parametric adaptation law was proposed and evaluated based on two 6-DOF industrial robots, showing better performance in maintaining the desired trajectory tracking even in the presence of large parametric uncertainties and external disturbances. Similarly, in [39], a combined robust adaptive control was designed by combining the robust term and the adaptive term, and in [40], an adaptive robust sliding-mode tracking controller was used for a 6 degree-of-freedom industrial assembly robot, where unknown parameter estimates were updated online based on a discontinuous projection adaptation law. In [41], an enhanced robust motion tracking control was synthesized by using disturbance adaption and modified iterative control terms, which better minimized the trajectory tracking errors in finite time. These works can achieve well tracking performance, but all of them focus on the interaction between the robot's arm and the environment, which cannot be implemented in the bimanual tasks, especially for the asymmetric cooperation control. As a result, the existing control techniques for the human–robot interaction do not provide much flexibility for collaboration tasks, requiring that the robot leads or follows the human by assessing the performance of the human in real time. The robot control scheme should be able to transit between the robot and human in the case of dominant roles.

Considering the auxiliary functions of the dual-arm exoskeleton and the tasks of human–human collaboration, we mainly investigate two cooperative manipulation models, that is: 1) the *following the better* model and 2) the *interpersonal goal integration* model, to illustrate the concept of asymmetric bimanual manipulation. We formulate a physical interaction in a continuous tracking task that takes advantage of both human knowledge and the robot's ability in a stable manner. Humans are able to respond intelligently to unpredictable changes in the real world and perform skilly in manipulation tasks. However, the existing control techniques for human–robot interaction have not provided sufficient flexibility for collaborative manipulation to leverage human guidance and the capabilities of robots. In this article, the region-based Barrier Lyapunov function (BLF) is designed to handle the change of roles between the human and the robot and ensures the operation within the constrained human and robot regions when driving the dual-arm exoskeleton to track the moving target.

We have done lots of research on asymmetric cooperation control of dual-arm exoskeletons. The works of Li *et al.* [15] and Huang *et al.* [18] focus on the human–robot skill transfer by adjusting the impedance parameters and interaction force with human sEMG signals. In [14] and [16], only interaction force and the position are considered as a communication medium between human arms and robot arms to obtain the motion intention of the human. Though they can achieve good performance in the interaction human–robot to a certain extent. However, the above works focus on the human-alone behavior (except for the last one), which does not consider the other human partners. Though the work of Wu and Li [16] refers to human partners interaction, the focus is on the tracking performance which does not mind the human–human cooperation with robot assistance. Moreover, the manipulation workspace of the human–exoskeleton system was not considered, which may influence the human–robot interaction performance (e. g., safety and manipulation compliance).

This article is an improvement and extension of our previous works on asymmetric cooperation control of dual-arm exoskeletons. In this article, two models, that is: 1) the following the better model and 2) the interpersonal goal integration model, are designed to facilitate the human–human collaborative manipulation. The nomenclatures including variables, parameters, and sets are provided in Table I. The contributions of this article are summarized as follows.

1) Two models have been proposed in which physically interacting humans are able to acquire information about the target's motion from the partner, that is: a) the *following the better model* and b) *the interpersonal goal integration model*. Therefore, the manipulation workspace for the human–exoskeleton system is divided into a human region and a robot region. In the human region, the human plays a more active role in the manipulation task, and in the robot region, the robot is more dominant in the manipulation. Compared to the learning-based method, we do not need too much prior knowledge and a complex learning process to be able to obtain the target's motion from the partner.
2) Based on the smooth combination of the human region and robot region, a unified expression is necessary to achieve the switching of the two regions. To address this issue, an adaptive tracking controller incorporating the novel region-based BLF has been designed to ensure the convergence of tracking errors in the presence of region switches, where the nonlinearities and uncertainties of the dynamics of the human and robot are considered.

II. Human–Human Collaborative Models

In our proposed task, there are two subjects and two exoskeleton arms, and each subject is equipped with an exoskeleton arm to track a moving target in the task space (Fig. 2). During the tracking task, each human wears an exoskeleton arm and the exoskeletons are individually controlled. First, subjects wearing exoskeleton arms track the moving target independently. The subject closer to the target is considered as a master, while the other subject is considered as a follower. We proposed two models, that is: 1) the *following the better* and 2) the *interpersonal goal integration* in task space. As the models are proposed in task space, there is only one configuration of the end effector in task space. In the model of *following the better*, the master is followed rather than the target, and in the model of *interpersonal goal integration*, the follower tracks the reference trajectory estimated from the haptic force between the master and the robot. The robots are designed to drive the master and the follower to track the moving target and the reference trajectory of the target, respectively. In the proposed controller, subjects are allowed to actively change the robot states in a small region for better tracing performance.

A. Dynamics of Task

Consider the task of tracking a moving target $T = [t, \dot{t}, \ddot{t}]^T \in \mathbb{R}^6$ with the position $t \in \mathbb{R}^2$, the velocity $\dot{t} \in \mathbb{R}^2$, and the acceleration $\ddot{t} \in \mathbb{R}^2$ in task space. The control input u that drives the human hand $X_h = [x_h, \dot{x}_h, \ddot{x}_h]^T \in \mathbb{R}^6$ to track the target state T takes the form of

$$u = -\left[K_p, K_v, K_a\right]\left[x_h - t, \dot{x}_h - \dot{t}, \ddot{x}_h - \ddot{t}\right]^T \tag{1}$$

which is the control law to move the hand toward the target, where $K = [K_p, K_v, K_a]$ is the control gain for the position, velocity, and acceleration.

The time derivation of T is

$$\dot{T} = AT + B\dddot{t} \tag{2}$$

where $A \in \mathbb{R}^{6\times6}$ and $B \in \mathbb{R}^{6\times2}$.

Consider two partners wearing two robotic exoskeletons, which are classified as the master and the follower, respectively. The human hand is modeled as a point-mass m with dynamics

$$m\ddot{x}_h = u + f_e \tag{3}$$

where $f_e \in \mathbb{R}^2$ is the interaction force between the human and exoskeleton which is assumed to be equal to the haptic force exerted by a human on the end effector and measurable by the force sensor. When wearing robotic exoskeletons, the

partner's hands coincide with the end effectors of the robotic exoskeletons.

Following (2) and (3), the dynamics of the hand $X_h = [x_h, \dot{x}_h, \ddot{x}_h]^T$ are described as

$$\dot{X}_h = AX_h + B\dddot{x}_h = AX_h + B\left(\dot{u}/m + \dot{f}_e/m\right). \tag{4}$$

Define the error vector $E = X_h - T = [e, \dot{e}, \ddot{e}]^T$ between the hand and the target. Based on (2)–(4), the error dynamics is

$$\dot{E} = AE + B\dddot{e} = AE + B\left(\dot{u}/m + \dot{f}_e/m - \dddot{t}\right). \tag{5}$$

B. Following the Better

The target position is assumed to be known to the robot and the exoskeleton robots drive the two partners to track the moving target. During target tracking, the master tracks the target while the follower tracks the master. Thus, the model is called *following the better*.

The observation depends on

$$e = \left[e_m, e_f\right]^T = \left[x_m - t, x_f - x_m\right]^T \tag{6}$$

where x_m and x_f denote the positions of the master and follower, respectively, and e_m, and e_f denote the tracking error of the master and follower, respectively.

C. Interpersonal Goal Integration

The proposed *interpersonal goal integration* model assumes that there is an impedance model between the master and the target, which produces the reference trajectory for his/her hand approaching the moving target by using f_e, and motor control drives the other partner's hand by the robotic exoskeleton following the reference trajectory [Fig. 2(b)]. This reference trajectory of the moving target produced by the impedance control between the master and the target is known to the exoskeleton robots.

The traditional mass-damper-spring model used to mimic both the hand and the moving target dynamics can be presented as

$$M_e\left(\ddot{x}_m - \ddot{\hat{t}}\right) + B_e\left(\dot{x}_m - \dot{\hat{t}}\right) + K_e\left(x_m - \hat{t}\right) = f_e \tag{7}$$

where M_e, B_e, and K_e are diagonal matrices representing the mass, damper, and stiffness matrices, respectively, $\hat{t}$ represents the estimated position of the target, f_e is the measured haptic force exerted by the master, and x_m represents the location of the hand in task space. Since the impedance model is mainly related with the damper and spring components, thus it can be simplified as

$$B_e\left(\dot{x}_m - \dot{\hat{t}}\right) + K_e\left(x_m - \hat{t}\right) = f_e \tag{8}$$

where B_e and K_e are impedance parameters. After the estimated trajectory of the target is obtained, the robot drives the partner to track the estimated trajectory.

Then, the *interpersonal goal integration* model is a combination of the partner goal and the estimation trajectory based on impedance model, such that

$$e = \left[e_m, e_f\right]^T = \left[x_m - t, x_f - \hat{t}\right]^T. \tag{9}$$

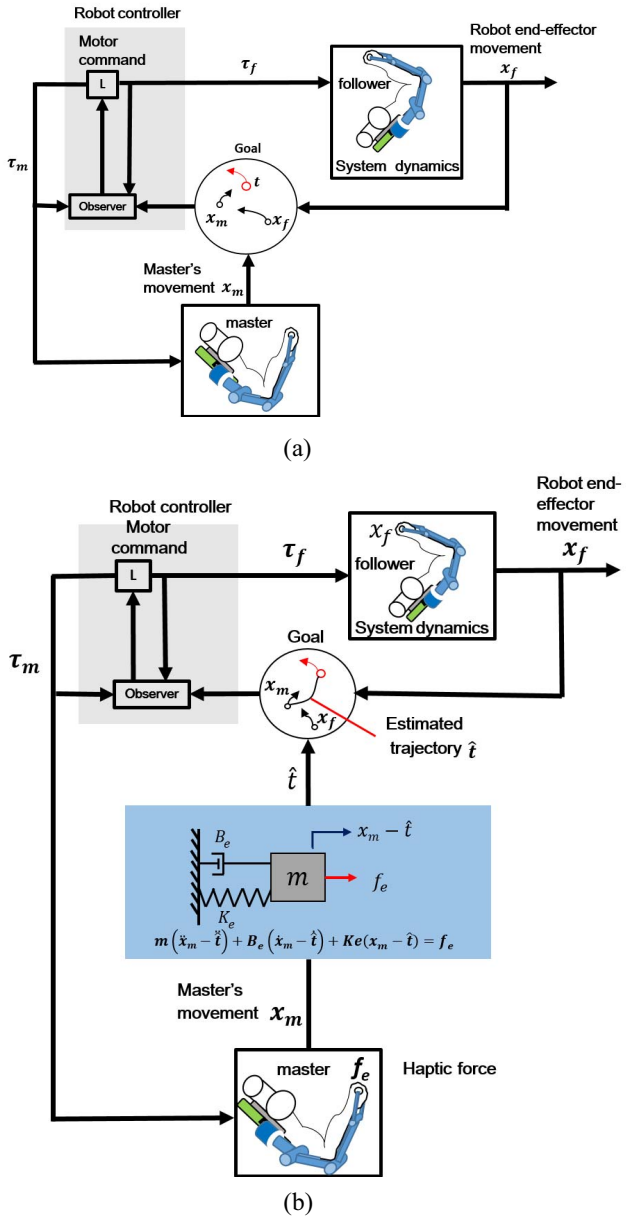

Fig. 2. (a) Model *following the better*. (b) Model *interpersonal goal integration*.

III. Kinematic and Dynamics of Dual-Arm Exoskeleton Robot

Considering the coupled system with the dual-arm exoskeleton and two partners acting as the master and the follower, respectively, the dynamics of the robot and the partners are described as

$$M_m(q_m)\ddot{q}_m + C_m(q_m, \dot{q}_m)\dot{q}_m + G_m(q_m) = \tau_m + \tau_{em} \tag{10}$$

$$M_f(q_f)\ddot{q}_f + C_f(q_f, \dot{q}_f)\dot{q}_f + G_f(q_f) = \tau_f + \tau_{ef} \tag{11}$$

where the subscripts m and f represent the master and the follower, respectively, $M_i(q_i) \in \mathbb{R}^{n\times n}$ denotes the inertia matrix that is symmetric and positive definite, $C_i(q_i) \in \mathbb{R}^{n\times n}$ represents the centrifugal and Coriolis torques, $G_i(q_i) \in \mathbb{R}^n$ is a vector of gravitational torque, $\tau_i \in \mathbb{R}^n$ represents a vector of

control input, and $\tau_{ei} \in \mathbb{R}^n$ denotes the torque exerted by the human.

Let $x_i \in \mathbb{R}^m$, $i = m, f$, represent the positions of robotic exoskeleton's end effector in the Cartesian space. Consider the robot kinematics

$$x_i = h_i(q_i) \tag{12}$$

where $q_i \in \mathbb{R}^n$ is the joint variable of the exoskeleton robot and $h_i(\cdot) \in \mathbb{R}^n \to \mathbb{R}^m$ denotes a nonlinear transformation describing the relation between joint space and Cartesian space. The Cartesian-space velocity of end effector $\dot{x}_i$ is related to the joint-space velocity $\dot{q}_i$ as

$$\dot{x}_i = J_i(q_i)\dot{q}_i \tag{13}$$

where $J_i(q_i) \in \mathbb{R}^{m\times n}$ is the Jacobian matrix from joint space to Cartesian space.

Through the forward kinematics (12) and the Jacobian (13), the joint space dynamics can be written in task space as

$$M_{xi}(x_i)\ddot{x}_i + C_{xi}(x_i, \dot{x}_i)\dot{x}_i + G_{xi}(x_i) = f_i + f_{ei} \tag{14}$$

where the coefficient matrices are defined as $M_{xi} = J_i{}^{-T}M_iJ_i{}^{-1}$, $G_{xi} = J_i{}^{-T}G_i$, $C_{xi} = J_i{}^{-T}(C_i - M_iJ_i{}^{-1}\dot{J}_i)J_i{}^{-1}$, $f_i = J_i{}^{-T}\tau_i$, and $f_{ei} = J_i^{-T}\tau_{ei}$ and f_i is the control input force, and f_{ei} denotes the external force exerted by human.

For simplicity, we consider only nonredundant ($m = n$) robot with known Jacobian J in this article. Henceforth, we consider $x_i \in \mathbb{R}^n$. Note that $J_i{}^{-1}$ and $J_i{}^{-T}$ are involved in (14) which may cause issues at the singularities of them. For $J_i{}^{-1}$, it is set by specifying the constrained region such that all singularities are outside of the constrained region. The following properties hold.

Property 1: The inertial matrix M_{xi} is positive definite.

Property 2: The matrix $\dot{M}_{xi} - 2C_{xi}$ is skew symmetric.

Property 3: The left-hand side of (14) can be linearly parameterized as

$$M_{xi}(x_i)\varphi_1 + C_{xi}(x_i, \dot{x}_i)\varphi_2 + G_{xi}(x) = \phi(\varphi_1, \varphi_2, x_i, \dot{x}_i)\theta \tag{15}$$

for any $\varphi_1, \varphi_2 \in \mathbb{R}^n$, where $\theta \in \mathbb{R}^l$ contains constant parameters and $\phi \in \mathbb{R}^{n\times l}$ is the known regressor function.

Assumption 1: The external force exerted by the human is bounded.

IV. Control Development and Stability Analysis

For the task that the two partners track a randomly moving target, the control objective can be described as follows. The model *following the better* assumes that the master is better at the tracking task and the follower needs to follow the trajectory of the master. The proposed *interpersonal goal integration* model assumes the master can estimate the partner's target based on visual feedback, and there exists an impedance model for both the master hand and the target, which can generate the reference trajectory approaching the target's movement. The generated reference trajectory can then be shared with the follower to drive the exoskeleton robot to track the target. The control framework of the proposed model is shown in Fig. 3.

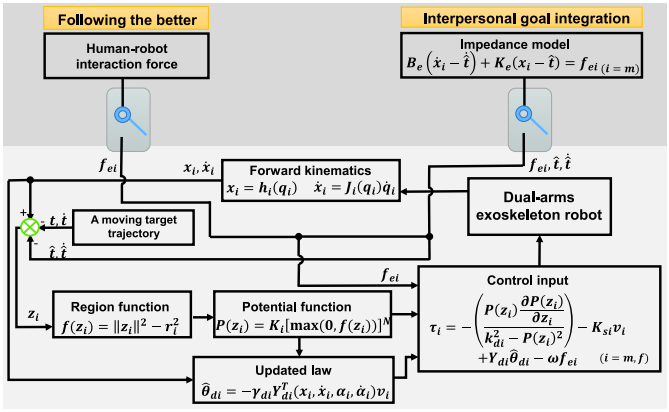

Fig. 3. Block diagram of human–human collaborative models including *following the better* and *interpersonal goal integration*. The subscript $i = m$ represents the master better at the tracking task, and the subscript $i = f$ represents the follower.

A. Human Region and BLF

According to the requirements of the tracking task, the two basic operating patterns of the controller include: 1) a human-dominant pattern, where the master's motions are encouraged and, therefore, only slightly interfered with by the robot system and 2) a robot-dominant mode, where the predefined desired movements can be fulfilled mostly by the robotic assistance.

The human-dominant mode refers to the situation that the better one or the master gains the free limb motion, and human motion control is trusted. In this case, it is important that the human limb can approach the moving target based on his vision and intention. At the same time, the system states remaining in the respective constraint sets can be guaranteed by using the BLF to avoid abnormal movements that may injure the participants; thus, the robotic exoskeleton can enhance the repeatability and accuracy of human motion control.

The robot-dominant mode represents the case that human motions are either unreliable or inefficient. Therefore, the assistance of the robot system is essential to either drive the human back to the right movements or finish the task, with the aim of driving the robot to the trajectory. Since the system can exhibit drift in position errors in performing tracking tasks, the generated torque can potentially cause damages to the participants. To address this issue, the operation space of the developed human–robot interaction model is divided into a human region and a robot region. In the human region, the human dominates without much interference by the robot. In the robot region, the human's effort is treated as a disturbance and will be eliminated by the robot.

Denote the errors as $z_i = x_i - x_{ri}$, $i = m, f$, where x_{ri} is the reference position in task space and x_i is the task variables. For the proposed *following the better* model, we choose $z_m = x_m - x_{rm}$, $x_{rm} = t$, and $z_f = x_f - x_{rf}$, $x_{rf} = x_m$, and for the *interpersonal goal integration* model, we choose $z_m = x_m - x_{rm}$, $x_{rm} = t$, and $z_f = x_f - x_{rf}$, $x_{rf} = \hat{t}$.

First, the human region is defined as

$$f(z_i) = \|z_i\|^2 - r_i^2 \le 0 \tag{16}$$

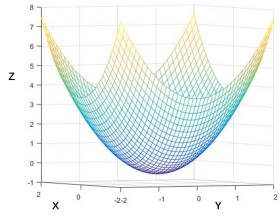

Fig. 4. Example of $f(z_i)$.

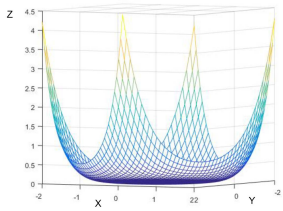

Fig. 5. Example of $P(z_i)$ when $N = 4$.

where $r_i \in \mathbb{R}^+$ denotes the radius of the human region. The value of r_i can be finely tuned according to different situations, and $f(z_i) \leq 0$ indicates the end effector is inside of the human region (Fig. 4), when the end effector is inside the human region, $f(z_i) \leq 0$, when the end effector is outside the human region, $f(z_i) > 0$. Then, the potential energy can be designed as

$$P(z_i) = K_i\big[\max(0, f(z_i))\big]^N \tag{17}$$

where K_i is a defined constant and N denotes the order of the function, which is an even integer.

Therefore, in this article, we proposed a BLF combined with the potential energy function to realize the switching of the human/robot-leading behavior. Unlike the traditional BLF [26], [27], which is directly based on the error z_i, in this article, we proposed a BLF combined with the potential energy function. When the position of the end effector is in the human region, the potential energy function $P(z_i)$ is equal to 0, which means that the human takes the lead while the robot only acts as compensation during the interaction behaviors when the position of the end effector is out of the human region, that is, in the robot region, the potential energy $P(z_i) > 0$ which means the robot acts as a leader until the end effector enters the human region. In Fig. 5, the bottom corresponds to $f(z_i) \leq 0$, that is, the end effector is inside the human region.

In this article, the error z_i is constrained as $\|z_i\|^2 < k_{ci}$ to avoid abnormal movement, where k_{ci} is a constant and $k_{ci} > r_i$. Since $P(z_i)$ increases with the increase of $\|z_i\|^2$, when the end effector is outside the human region, $\|z_i\|^2 < k_{ci}$ is equivalent to $P(z_i) < k_{di}$, where k_{ci} and k_{di} are positive constants.

To ensure that z_i satisfies the constraint, we employ a BLF, whose value approaches infinity as its arguments approach some limits. The BLF based on the potential energy $P(z_i)$ is proposed as

$$V_1 = \frac{1}{2}\ln\left(\frac{{k_{di}}^2}{{k_{di}}^2 - P(z_i)^2}\right). \tag{18}$$

The value of V_1 approaches infinity as $P(z_i) \to k_{di}$. The time derivative of V_1 is given by

$$\dot{V}_1 = \frac{P(z_i)\left(\frac{\partial P(z_i)}{\partial z_i}\right)^T(\dot{x}_i - \dot{x}_{ri})}{k_{di}^2 - P(z_i)^2}. \tag{19}$$

Denoting the vector $v_i = \dot{x}_i - \alpha_i$, where α_i is a stabilizing function to be designed, then $\dot{x}_i = v_i + \alpha_i$. The time derivative can be rewritten as

$$\dot{V}_1 = \frac{P(z_i)\left(\frac{\partial P(z_i)}{\partial z_i}\right)^T(v_i + \alpha_i - \dot{x}_{ri})}{k_{di}^2 - P(z_i)^2}. \tag{20}$$

Letting $\alpha_i = \dot{x}_{ri} - \beta\frac{\partial P(z_i)}{\partial z_i}$, then we have

$$\dot{V}_1 = \frac{P(z_i)\left(\frac{\partial P(z_i)}{\partial z_i}\right)^T\left(v_i - \beta\frac{\partial P(z_i)}{\partial z_i}\right)}{k_{di}^2 - P(z_i)^2} \tag{21}$$

where β is a positive constant.

Using the vector v_i and the properties of robot dynamics, the robot dynamics described in (14) can be written as

$$M_{xi}(x_i)\dot{v}_i + C_{xi}(x_i, \dot{x}_i)v_i + Y_{di}\big(x_i, \dot{x}_f, \alpha_i, \dot{\alpha}_i\big)\theta_{di} = f_i + f_{ei} \tag{22}$$

where $Y_{di}(x_i, \dot{x}_i, \alpha_i, \dot{\alpha}_i)\theta_{di} = M_{xi}(x_i)\dot{\alpha}_i + C_{xi}(x_i, \dot{x}_i)\alpha_i + G_{xi}(x_i)$. In the presence of uncertain robot dynamics, the vector of the dynamic parameters θ_{di} is unknown such that

$$Y_{di}(x_i, \dot{x}_i, \alpha_i, \dot{\alpha}_i)\hat{\theta}_{di} = \hat{M}_{xi}(x_i)\dot{\alpha}_i + \hat{C}_{xi}(x_i, \dot{x}_i)\alpha_i + \hat{G}_{xi}(x_i) \tag{23}$$

where $\hat{\theta}_{di}$ denotes the estimate of θ_{di}, and $\hat{M}_{xi}(x_i)$, $\hat{C}_{xi}(x_i, \dot{x}_i)$, and $\hat{G}_{xi}(x_i)$ represent the approximate model for $M_{xi}(x_i)$, $C_{xi}(x_i, \dot{x}_i)$ and $G_{xi}(x_i)$, respectively, and the uncertain parameter $\hat{\theta}_{di}$ is updated by

$$\dot{\hat{\theta}}_{di} = -\gamma_{di}Y_{di}^T(x_i, \dot{x}_i, \alpha_i, \dot{\alpha}_i)v_i \tag{24}$$

where γ_{di} denotes the control gain of adaptation, which is also a positive-definite matrix.

Consider the Lyapunov Function candidate as

$$V_2 = V_1 + \frac{1}{2}v_i^T M_{xi}(x_i)v_i + \frac{1}{2}\Delta\theta_{di}^T\gamma_{di}^{-1}\Delta\theta_{di} \tag{25}$$

where $\Delta\theta_{di} = \theta_{di} - \hat{\theta}_{di}$. The time derivative of V_2 is

$$\dot{V}_2 = v_i^T M_{xi}(x_i)\dot{v}_i + \frac{1}{2}v_i^T\dot{M}_{xi}(x_i)v_i - \Delta\theta_{di}^T\gamma_{di}^{-1}\dot{\hat{\theta}}_{di} + \dot{V}_1. \tag{26}$$

Substituting (22)–(25) into (26) and using the properties of robot dynamics, we have

$$\begin{aligned}\dot{V}_2 &= v_i^T\big[-Y_{di}(x_i, \dot{x}_i, \alpha_i, \dot{\alpha}_i)\theta_{di} + f_i + f_{ei}\big] \\ &\quad - \Delta\theta_{di}\gamma_{di}^{-1}\dot{\hat{\theta}}_{di} + \dot{V}_1 \\ &= v_i^T\big[-Y_{di}(x_i, \dot{x}_i, \alpha_i, \dot{\alpha}_i)\theta_{di} + f_i + f_{ei}\big] - \Delta\theta_{di}^T\gamma_{di}^{-1}\dot{\hat{\theta}}_{di} \\ &\quad + \frac{P(z_i)\left(\frac{\partial P(z_i)}{\partial z_i}\right)^T\left(v_i - \beta\frac{\partial P(z_i)}{\partial z_i}\right)}{k_{di}^2 - P(z_i)^2}.\end{aligned} \tag{27}$$

Design the control law as

$$f_i = g_i - K_{si}v_i + Y_{di}\hat{\theta}_{di} - \omega f_{ei} \tag{28}$$

where

$$g_i = -\left(\frac{P(z_i)\frac{\partial P(z_i)}{\partial z_i}}{k_{di}{}^2 - P(z_i)^2}\right)$$

and $\omega = 0$ when the end effector is inside of the human region and $\omega = 1$ when the end effector is outsider of the human region. When the end effector is inside of the human region, $g_i = 0$ because of $P(z_i) = 0$, then the control law can be rewritten as

$$f_i = -K_{si}v_i + Y_{di}\hat{\theta}_{di} \tag{29}$$

Then, $\dot{V}_2$ can be rewritten as

$$\dot{V}_2 = -v_i^T K_{si} v_i + v_i^T(1-\omega)f_{ei} - \frac{\beta P(z_i)\left\|\frac{\partial P(z_i)}{\partial z_i}\right\|^2}{k_{di}^2 - P(z_i)^2}. \tag{30}$$

Then, we need to state the boundedness of vector v_i. Let

$$W_i = v_i^T K_{si} v_i + \frac{\beta P(z_i)\left\|\frac{\partial P(z_i)}{\partial z_i}\right\|^2}{k_{di}^2 - P(z_i)^2}$$

which is non-negative, (30) can be rewritten as

$$\dot{V}_2 = -W_i + v_i^T(1-\omega)f_{ei}. \tag{31}$$

Integrating (31) over $[0, t]$ yields

$$\int_0^t v_i^T(\varsigma)(1-\omega)f_{ei}(\varsigma)d\varsigma = V_2(t) - V_2(0) + \int_0^t W_i(\varsigma)d\varsigma. \tag{32}$$

It should be noted that

$$\int_0^t v_i^T(\varsigma)(1-\omega)f_{ei}(\varsigma)d\varsigma \le \frac{1}{2}\int_0^t \|v_i(\varsigma)\|^2 d\varsigma + \frac{1}{2}\int_0^t \|(1-\omega)f_{ei}(\varsigma)\|^2 d\varsigma. \tag{33}$$

Since V_2 is positive, we have

$$-V(0) + \int_0^t W_i(\varsigma)d\varsigma \le \frac{1}{2}\int_0^t \|v_i(\varsigma)\|^2 d\varsigma + \frac{1}{2}\int_0^t \|(1-\omega)f_{ei}(\varsigma)\|^2 d\varsigma. \tag{34}$$

If K_{si} is chosen large enough such that

$$\frac{1}{\delta^2} \triangleq 2\lambda_{\min}(K_{si}) - 1 > 0 \tag{35}$$

where $\delta > 0$, and $\lambda_{\min}(K_{si})$ denotes the minimum eigenvalue. Since W_i is non-negative, substituting W_i into (34) yields

$$(2\lambda_{\min}(K_{si}) - 1)\int_0^t \|v_i(\varsigma)\|^2 d\varsigma \le \int_0^t \|(1-\omega)f_{ei}(\varsigma)\|^2 d\varsigma + 2V_2(0). \tag{36}$$

Then, using (35), we have

$$\int_0^t \|v_i(\varsigma)\|^2 d\varsigma \le \delta^2\left(\int_0^t \|(1-\omega)f_{ei}(\varsigma)\|^2 d\varsigma + 2V_2(0)\right). \tag{37}$$

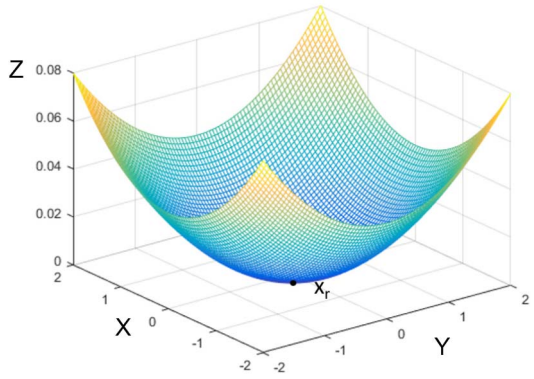

Fig. 6. Radius of human region is set to 0, x_r denotes the reference position.

If the initial position lies in the constrained region, that is, $P(z_i(0)) < k_{di}$, $V_2(0)$ is bounded. f_{ei} is bounded according to Property 3. Therefore, v_i is bounded. Since v_i is bounded and $v_i = \dot{x}_i - \alpha_i$, the boundedness of v_i ensures the boundedness of task space velocity $\dot{x}_i$.

Since $([\partial P(z_i)/[\partial z_i]) \neq 0$ when $0 < P(z_i) < k_{di}$, then $-([\beta P(z_i)\|\partial P(z_i)/\partial z_i\|^2]/[k_{di}^2 - P(z_i)^2]) < 0$ when $0 < P(z_i) < k_{di}$. At this time, the end effector is outside the human region, then we have

$$\dot{V}_2 = -v_i K_{si} v_i - \frac{\beta P(z_i)\left\|\frac{\partial P(z_i)}{\partial z_i}\right\|^2}{k_{di}^2 - P(z_i)^2} \le 0. \tag{38}$$

Since $V_2(0)$ is bounded and $\dot{V}_2 \le 0$, it can be shown that V_2 is bounded $\forall t > 0$. According to (18), V_1 is bounded, and the potential energy $P(z_i)$ remains in the region $P(z_i) < k_{di}$ $\forall t > 0$. According to [20], it is concluded that $P(z_i) \to 0$ as $t \to \infty$. From the definition of $P(z_i)$, $P(z_i) = 0$ implies the end effector is controlled to move to the inside of the human region. When the end effector is inside the human region, the control input is $f_i = -K_{si}(\dot{x}_i - \dot{x}_{ri}) + Y_{di}\hat{\theta}_{di}$.

If the radius of the human region is set to 0 (Fig. 6), the reference position x_{ri} is the time-varying trajectory. Based on the analysis above, $P(z_i) \to 0$ as $t \to \infty$ indicates $x_i \to x_{ri}$. In other words, the robot drives the participants to track x_{ri}.

V. Experiments Verification

A. System Description

Several experiments were performed on an exoskeleton system to demonstrate the functionality and performance of the proposed controller in performing asymmetric cooperative tasks and how two partners cooperate with each other during the two proposed models. A double-arm exoskeleton robot consisting of two 6-DOF exoskeleton arms is developed for laboratory experiments, as shown in Fig. 1. Decentralized control for two arms of the exoskeleton is utilized, that is, two computers to control two arms of the exoskeleton robot, respectively, and the communication between the two computers is allowed during the experiments. The kinematics of the exoskeleton is similar to the upper limb of the human. Moreover, the experimental setup still includes a monitor that

TABLE II
INFORMATION OF THE SUBJECTS

Group	Experimenter	Age	Weight	FIM	Results
Group 1	Subject 1	25(female)	53kg	120	Fig. 8-24
	Subject 2	25(male)	81kg	123	
Group 2	Subject 1	26(female)	52kg	116	
	Subject 2	26(male)	85kg	119	
Group 3	Subject 1	24(female)	47kg	125	
	Subject 2	24(male)	74kg	122	

provides position information of targets for humans and partners. The humans are positioned and can observe each other by their visual feedback on the monitor. There may be a lag in the observed position information, but the robot's assistance will compensate for it. In the developed exoskeleton, there is a high-resolution encoder (2048 pulse/cycle) for each joint and a hall effect sensor for position sensing and measurement. The exoskeleton robot is developed with the dc motor as the actuator, and Maxon dc flat brushless motor EC45 is chosen as the driver unit. A six-axis force sensor is installed between the end actuator and the bracket to measure the interaction force between the robot and human. The human and the robot cooperate to complete the specified task in the x–y plane.

A four-layer control architecture in the dual-arm exoskeleton includes a control computer, servo motor, motor driver (Elmo driver), and exoskeleton. The setup of the exoskeleton is shown in Fig. 1, where the desired messages, such as the position and angular velocity, can be read from the joint sensors and generate a power signal to activate the actuator. A computer running WinXP is chosen as the control unit. The developed control architecture consists of three components: 1) the exoskeleton for sensing and actuation; 2) a motion unit performing as the lower controller to generate a driving force for the exoskeleton joints, nominally running at 1 kHz; and 3) the display of application development and control graphics on the host computer, nominally updated with 100 Hz. The low-level controller is connected to the Windows XP PC by the ELMO driver through the CAN bus to implement the real-time control. The control application of the exoskeleton is realized in the Win XP environment based on the CAN network. Visual C++ was used for experimental software development. The graphical interface shows position sensing signals and can be used to tune control parameters in experimental trials. An experimental interface is developed to show the progress of experiments. To demonstrate the feasibility of the proposed strategy, three groups of subjects are involved in the experiment, as shown in Table II. The subjects of each group chosen are the people with muscle damage or some degree of motor dysfunction. The functional independence measure (FIM) can be seen in Table II. It should be noted that the cognitive functions of the subjects in the experiment have no cognitive impairment.

During the experiment, the subject wears one of the two arms of the exoskeleton robot and holds the end effector, and completes the tracking task with a cooperative partner. For the experiment employed, the subjects have provided the corresponding informed consent, with the approval of the university.

B. Experiment Description

The purpose of the experiments was to test the performance of the controller. Several experiments were carried out on the exoskeleton robot in Fig. 1. Specifically, two different experiments involved stand-alone trials with one subject controlling the exoskeleton robot and connected trials with two subjects controlling the robot separately. Among them, the stand-alone task is one of the important procedures to demonstrate the validity of the proposed controller (the region-based BLF controller). Therefore, we set as a group of comparison experiments on the stand-alone task, where the first stand-alone trial is a passive tracking trajectory without a human involved and the second one is a subject with the assistance of the exoskeleton robot tracked the moving target itself. Then, the connected trials corresponded to the two models mentioned above. The first connected experiment was called *following the better*, and the second one called *interpersonal goal integration*. These experiments were conducted and the performance indices used to measure the quality of the human cooperative control include the following.

1) The average tracking error $L_2[e] = \sqrt{(1/T_f)\int_0^{T_f} |e|^2 dt}$ where T_f represents the total running time.
2) The average control input $L_2[\tau] = \sqrt{(1/T_f)\int_0^{T_f} |\tau|^2 dt}$.

In the experiment, the following parameters were used: $K_{si} = \text{diag}[0.1, 0.1]$, $\beta = 0.1$, $\gamma_{di} = \text{diag}[1e-5, 1e-5]$, the initial parameters are chosen as $\hat{\theta}_{di} = [\hat{\theta}_{di1}, \hat{\theta}_{di1}] = [0.0, 0.0]^T$, and the order of the potential energy is selected as $N = 4$ and we choose $K_i = 3.2$, $K_{ci} = 0.0025$, $K_{di} = 0.0125$, and the upper limb exoskeleton robot is shown in Fig. 1 with the length of two links as $l_1 = 0.32$ m and $l_2 = 0.28$ m, respectively. Four sets of experiments were conducted. In the first experiment, the robot tracked a moving target. In the second experiment, the robot and a partner cooperatively tracked the moving target. In the last two experiments, the developed *following the better* model and the *interpersonal goal integration* model were applied, respectively.

In the first stand-alone experiment, when the robot tracked the moving target, the human region was set to 0 and the safe region is set to 0.08 m. The experimental results are shown in Fig. 7(a) and (b). From the experimental result, we can see that the tracking error is fairly small and the robot is within the safe region, where $\|z_1\|$, $\|z_2\|$, and $\|z_3\|$ denote the tracing error of every group. In the second stand-alone experiment, the robot tracked the moving target, the human region was set to 0.04 m, and the robot region is 0.08 m. The results of the experiment are shown in Figs. 7(c) and 8.

C. Experiment on Following the Better

The first connected experiment verified the model of *following the better* [see Fig. 2(a)]. The radius of the human region r_i was chosen as 0.04 m for the follower and 0.04 m for the master and the safe region is set to 0.08 m for every group. The master tracked the moving target while the follower was driven by the robot to follow the trajectory of the master. The experimental result in task space is shown in Fig. 9(a)

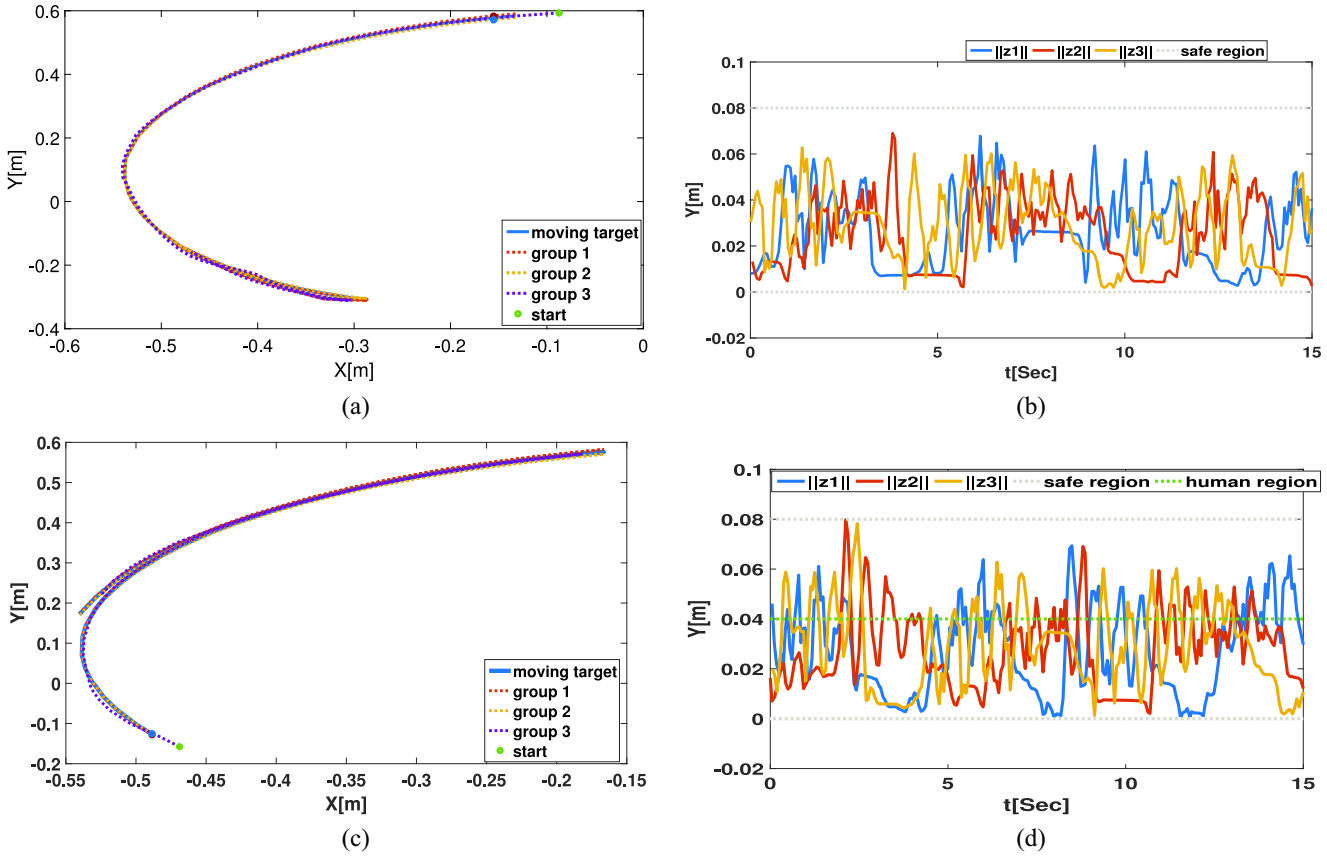

Fig. 7. (a) Trajectories of the moving target and the actual trajectories of group 1, group 2, group 3 without a human involved. (b) Tracking error of each subject. (c) Trajectories of the moving target and the actual trajectories of group 1, group 2, and group 3 with a subject involved. (d) Tracking error of every group.

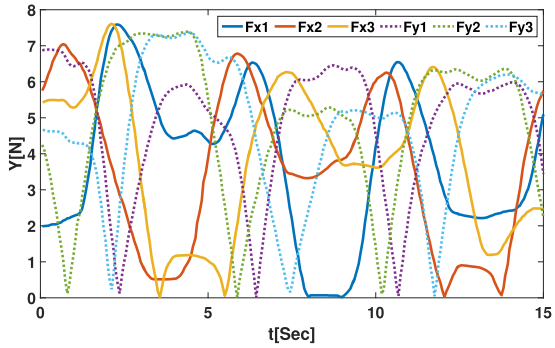

Fig. 8. Interaction force of the second experiment, where F_{x1} and F_{y1} denote the interaction force of group1, F_{x2} and F_{y2} denote the interaction force of group 2 and F_{x3} and F_{y3} denote the interaction force of group 3.

TABLE III
AVERAGE TRACKING ERROR AND CONTROL INPUT

Experiments	EX 1	EX 2	EX 3	EX 4
Average tracking error (m)	0.03036	0.04227	0.03664	0.03655
Average control input (A)	2.1444	1.8993	1.9102	1.9085

and (b). Fig. 9(c) and (d) shows the errors of the model *following the better* and Fig. 9(e) and (f) shows the interaction force.

D. Experiment on Interpersonal Goal Integration

The second connected experiment verified the model of *interpersonal goal integration* in Fig. 2(b), where the master exerted force on the end effector of the exoskeleton and the trajectory of the moving target was estimated from the haptic force exerted by the master through the impedance model between the moving target and the end effector. After the trajectory was obtained, the exoskeleton robot drove the follower to track the estimated trajectory. During the experiment, the haptic force was applied according to the visual feedback of the master, and the force was measured by the force sensor mounted on the end actuator, and r_i is set as 0.04 m. The safe region is set as 0.08 m. The robot with the master tracked the moving target is shown in Fig. 10(a). Meanwhile, the estimated trajectory was transferred to the exoskeleton with the follower, and the robot drove the follower to track the transferred trajectory in Fig. 10(b) and (d). Fig. 10(e) and (f) shows the tracking errors of the master and follower of the model *interpersonal goal integration*. Fig. 7(a) and (b) shows the interaction force.

E. Discussion

From the experimental results, we can see that the robot was within the safe region and the subjects can track the moving target in each experiment. Table III shows the control inputs and the tracking error of the four experiments. The

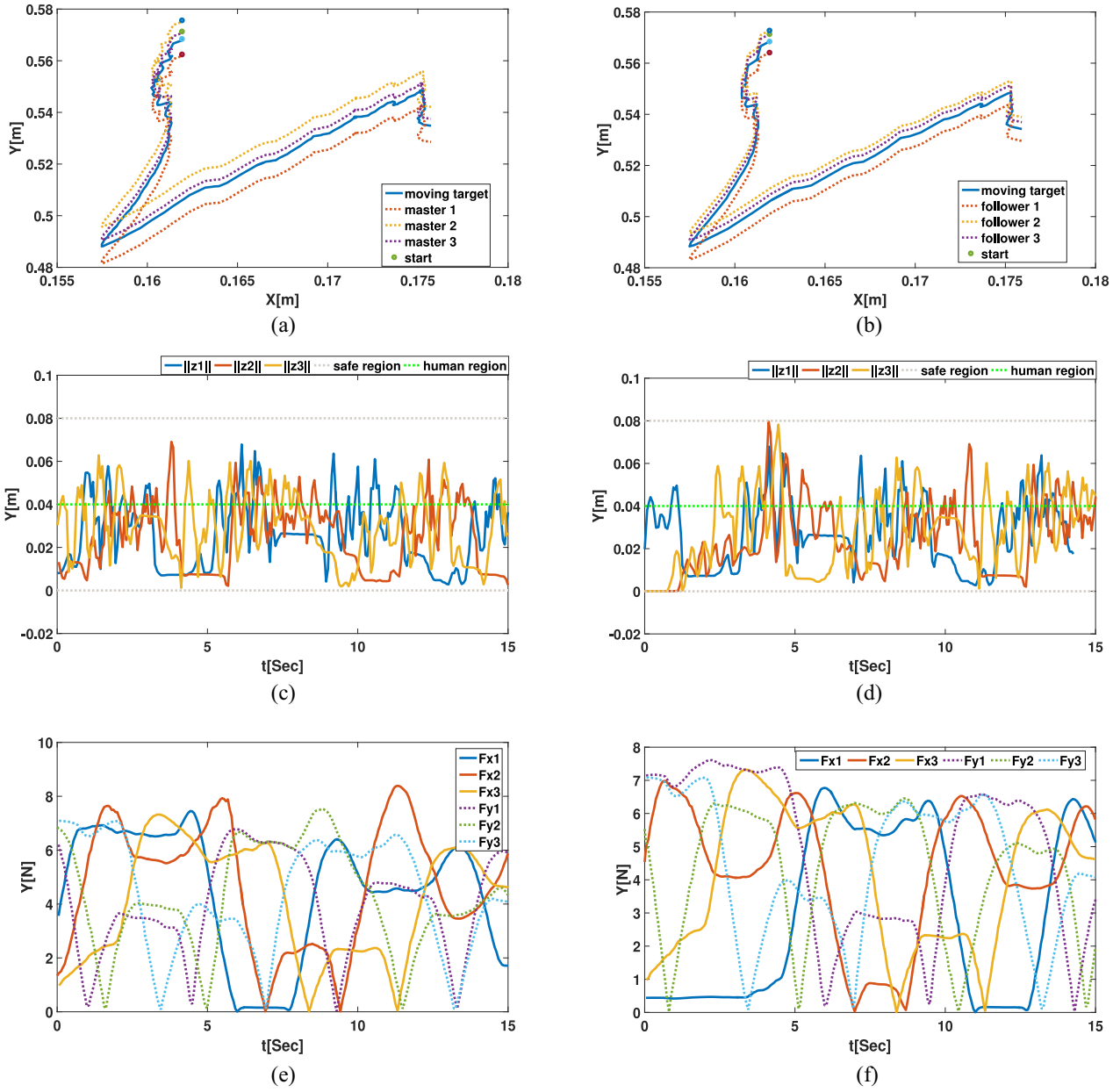

Fig. 9. (a) and (b) Trajectories of the moving target, master and follower in task space. (c) Tracking errors of the model *following the better* by the master. (d) Tracking errors of the model *following the better* by the follower. (e) Interaction force of the model *following the better* by the master. (f) Interaction force of the model *following the better* by the follower.

comparison shows that the control input of the experiments with humans was smaller than that without humans, because in a human cooperative control strategy, when the robot is in the human region, one can change the state of robots, and the control input of robots is reduced. Figs. 8, 9(e) and (f), and 10(g) and (h) show the interaction forces. The first experiment has the best tracking performance because the fixed trajectory of the moving target was tracked and the control input of the first experiment is the largest as the subject is driven by the robot passively. The average tracking error of the second experiment is larger than our proposed models. As shown in Table IV, for every stand-alone experiment, the average tracing error is similar.

Although the proposed approach paves the way for multihuman–robot interaction systems, there are some limitations. For example, the region radius cannot be adjusted and the region switching point cannot be planned online in real time, that is, when the subjects need more freedom to adjust their posture to track the target better, the robot can allow and give the subjects more initiative in a timely manner.

In the experiments, since the parameters may not be applicable to all the partners with different ages, stature, and motion

TABLE IV
AVERAGE TRACKING ERROR OF EACH GROUP (M)

Experiments	EX 1	EX 2	EX 3	EX 4
Group 1	0.03036	0.04227	0.03664	0.03655
Group 2	0.03004	0.04425	0.0385	0.03555
Group 3	0.03019	0.04223	0.03781	0.03583

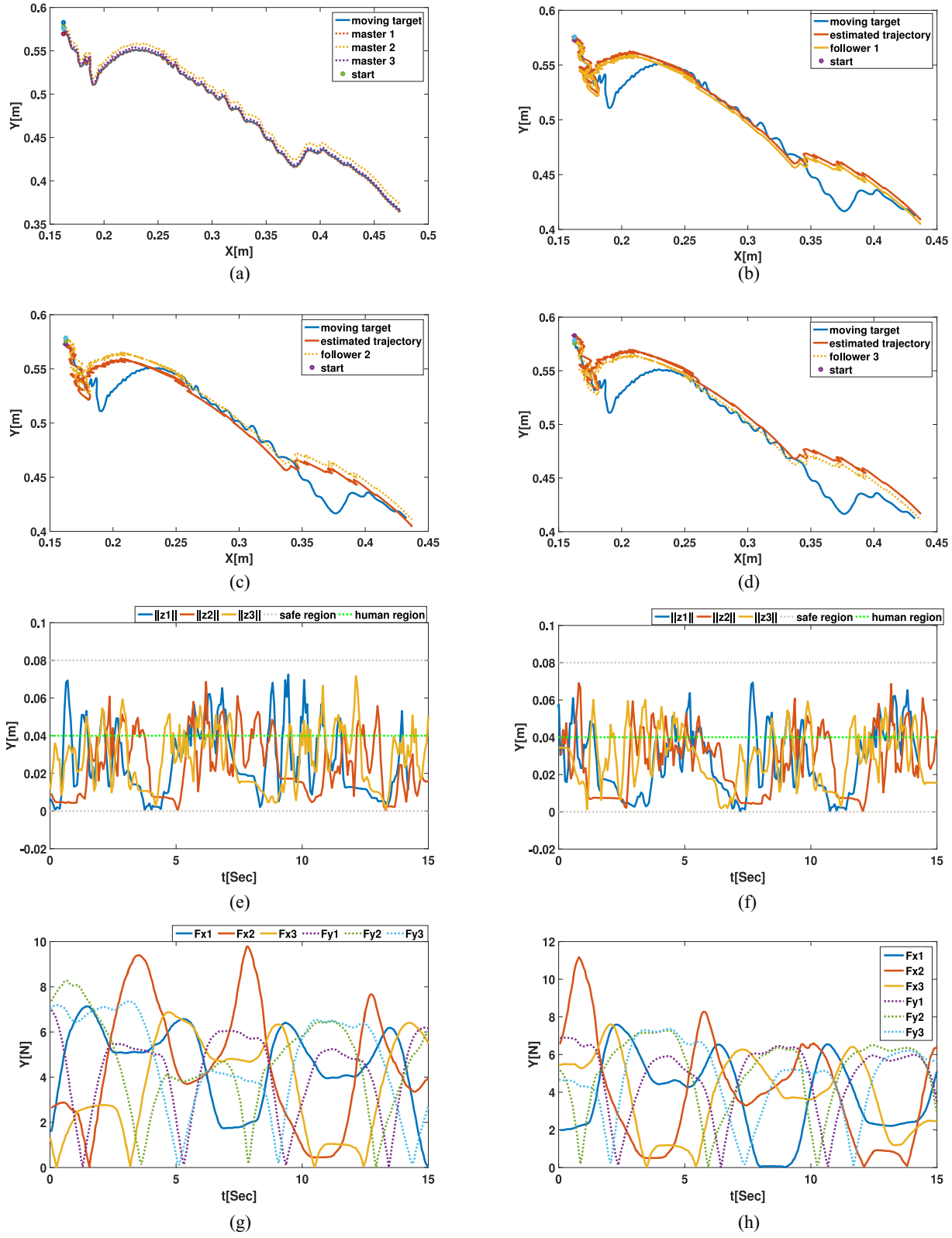

Fig. 10. (a) Trajectories of the moving target master of every group. (b) Trajectories of the moving target, master, and follower of the first group. (c) Trajectories of the moving target, master, and follower of the second group. (d) Trajectories of the moving target, master, and follower of the third group. (e) Tracking errors of the master in *interpersonal goal integration*. (f) Tracking errors of the follower in *interpersonal goal integration*. (g) Interaction force of the model *interpersonal goal integration* by the master. (h) Interaction force of the model *interpersonal goal integration* by the follower.

capabilities, therefore, the parameters should provide flexibility for fine tuning or adjustment in experiments. When implementing this controller on an upper limb exoskeleton robot, the tuning of the parameter should consider the subjects' condition. If the parameter of human region r_i is chosen as 0 m, the subject performs passively and the robot drives

him/her to track the reference trajectory, and the external force applied by the subject is rejected by the controller. In the experiments, if more free motion is desirable for the subject, the radius of the human region should be increased and then we chose $r_i = 4$ cm.

Other parameters K_{ci}, K_{di}, K_{si}, and γ_{di} should be fine tuned and then fixed or limited to a small fine-tuning zone during the experiment. The selection of K_{ci} and K_{di} should consider the maximum torque that the human can bear and the motion of the participants because the motion of the robot may reach a condition that is harmful to the participants. Then, K_{si} is fine tuned to achieve the desired region tracking and steady-state error performance of the controller. Finally, the parameter adaption gain γ_{di} should start with small values and enlarge when a faster adaption is expected.

VI. Conclusion

In this article, two cooperative manipulation models were developed, that is: 1) the *following the better* and 2) *interpersonal goal integration* models. The models were implemented on the upper limb exoskeleton robots. The task space was divided into a human and a robot region. The radius of the human region can be tuned. We have proposed a novel region-based BLF to drive the dual-arm exoskeleton to track the moving target by each arm within the constrained regions. By using the Lyapunov analysis, we proved the closed-loop system is stable. The experimental results are presented to demonstrate the proposed models and the proposed controller. Compared to the human cooperative manipulation with only one partner, our proposed models have better tracking performance.

References

[1] R. Bertani, C. Melegari, M. C. De Cola, A. Bramanti, P. Bramanti, and R. S. Calabrò, "Effects of robot-assisted upper limb rehabilitation in stroke patients: A systematic review with meta-analysis," *Neurol Sci.*, vol. 38, no. 9, pp. 1561–1569, Sep. 2017.

[2] M. Babaiasl, S. H. Mahdioun, P. Jaryani, and M. Yazdani, "A review of technological and clinical aspects of robot-aided rehabilitation of upper-extremity after stroke," *Disabil. Rehabil. Assist. Technol.*, vol. 11, no. 4, pp. 263–280, 2016.

[3] D. Ao, R. Song, and J. Gao, "Movement performance of human-robot cooperation control based on EMG-driven hill-type and proportional models for an ankle power-assist exoskeleton robot," *IEEE Trans. Neural Syst. Rehabil. Eng.*, vol. 25, no. 8, pp. 1125–1134, Aug. 2017.

[4] H. S. Nam *et al.*, "Biomechanical reactions of exoskeleton neurorehabilitation robots in spastic elbows and wrists," *IEEE Trans. Neural Syst. Rehabil. Eng.*, vol. 25, no. 11, pp. 2196–2203, Nov. 2017.

[5] J. Huang, W. Huo, W. Xu, S. Mohammed, and Y. Amirat, "Control of upper-limb power-assist exoskeleton using a human-robot interface based on motion intention recognition," *IEEE Trans. Autom. Sci. Eng.*, vol. 12, no. 4, pp. 1257–1270, Oct. 2015.

[6] A. Takagi, G. Ganesh, T. Yoshioka, M. Kawato, and E. Burdet, "Physically interacting individuals estimate the partner's goal to enhance their movements," *Nat. Human Behav.*, vol. 1, no. 3, p. 54, Mar. 2017.

[7] K. B. Reed and M. A. Peshkin, "Physical collaboration of human-human and human-robot teams," *IEEE Trans. Haptics*, vol. 1, no. 2, pp. 108–120, Jul.–Dec. 2008.

[8] R. Groten, D. Feth, H. Goshy, A. Peer, D. A. Kenny, and M. Buss, "Experimental analysis of dominance in haptic collaboration," in *Proc. 18th IEEE Int. Symp. Robot Human Interact. Commun.*, 2009, pp. 723–729.

[9] R. P. R. D. van der Wel, G. Knoblich, and N. Sebanz, "Let the force be with us: Dyads exploit haptic coupling for coordination," *J. Exp. Psychol. Human Percept. Perform.*, vol. 37, no. 5, pp. 1420–1431, Oct. 2011.

[10] A. Sawers and L. H. Ting, "Perspectives on human-human sensorimotor interactions for the design of rehabilitation robots," *J. NeuroEng. Rehabil.*, vol. 11, pp. 1–13, Oct. 2014.

[11] K. Reed, M. Peshkin, M. J. Hartmann, M. Grabowecky, J. Patton, and P. M. Vishton, "Haptically linked dyads: Are two motor-control systems better than one," *Psychol. Sci.*, vol. 17, no. 5, pp. 365–366, 2006.

[12] S. O. Oguz, A. Kucukyilmaz, T. M. Sezgin, and C. Basdogan, "Haptic negotiation and role exchange for collaboration in virtual environments," in *Proc. IEEE Haptics Symp.*, 2010, pp. 371–378.

[13] S. Gentry, E. Feron, and R. Murray-Smith, "Human-human haptic collaboration in cyclical Fitts' tasks," in *Proc. IEEE/RSJ Int. Conf. Intell. Robots Syst.*, 2005, pp. 3402–3407.

[14] Z. Li, B. Huang, A. Ajoudani, C. Yang, C. Y. Su, and A. Bicchi, "Asymmetric bimanual control of dual-arm exoskeletons for human-cooperative manipulations," *IEEE Trans. Robot.*, vol. 34, no. 1, pp. 264–271, Feb. 2018.

[15] Z. Li, C. Xu, Q. Wei, C. Shi, and C.-Y. Su, "Human-inspired control of dual-arm exoskeleton robots with force and impedance adaptation," *IEEE Trans. Syst., Man, Cybern., Syst.*, vol. 50, no. 12, pp. 5296–5305, Dec. 2020.

[16] X. Wu and Z. Li, "Cooperative manipulation of wearable dual-arm exoskeletons using force communication between partners," *IEEE Trans. Ind. Electron.*, vol. 67, no. 8, pp. 6629–6638, Aug. 2020.

[17] A. M. Dollar and H. Herr, "Lower extremity exoskeletons and active orthoses: Challenges and state-of-the-art," *IEEE Trans. Robot.*, vol. 24, no. 1, pp. 144–158, Feb. 2008.

[18] B. Huang, Z. Li, X. Wu, A. Ajoudani, A. Bicchi, and J. Liu, "Coordination control of a dual-arm exoskeleton robot using human impedance transfer skills," *IEEE Trans. Syst., Man, Cybern., Syst.*, vol. 49, no. 5, pp. 954–963, May 2019.

[19] M. N. Ayala and D. Y. P. Henriques, "Context-dependent concurrent adaptation to static and moving targets," *PLoS One*, vol. 13, no. 2, 2018, Art. no. e0192476.

[20] X. Li, G. Chi, S. Vidas, and C. C. Cheah, "Human-gided robotic comanipulation: Two illustrative scenarios," *IEEE Trans. Control Syst. Technol.*, vol. 24, no. 5, pp. 1753–1763, Sep. 2016.

[21] E. Noohi, M. Zefran, and J. L. Patton, "A model for human-human collaborative object manipulation and its application to human-robot interaction," *IEEE Trans. Robot.*, vol. 32, no. 4, pp. 880–896, Aug. 2016.

[22] H. Kim *et al.*, "Kinematic data analysis for post-stroke patients following bilateral versus unilateral rehabilitation with an upper limb wearable robotic system," *IEEE Trans. Neural Syst. Rehabil. Eng.*, vol. 21, no. 2, pp. 153–164, Mar. 2013.

[23] S. Contu, C. M. L. Hughes, and L. Masia, "The role of visual and haptic feedback during dynamically coupled bimanual manipulation," *IEEE Trans. Haptics*, vol. 9, no. 4, pp. 536–547, Oct.–Dec. 2016.

[24] J. Oosterhout, C. J. M. Heemskerk, M. R. de Baar, F. C. T. van der Helm, and D. A. Abbink, "Tele-manipulation with two asymmetric slaves: Two operators perform better than one," *IEEE Trans. Haptics*, vol. 11, no. 1, pp. 128–139, Jan.–Mar. 2018.

[25] E. Gribovskaya, A. Kheddar, and A. Billard, "Motion learning and adaptive impedance for robot control during physical interaction with humans," in *Proc. IEEE Int. Conf. Robot. Autom.*, May 2011, pp. 4326–4332.

[26] K. P. Tee, S. S. Ge, and E. H. Tay, "Barrier Lyapunov functions for the control of output-constrained nonlinear systems," *Automatica*, vol. 45, no. 4, pp. 918–927, 2009.

[27] W. He, B. Huang, Y. Dong, Z. Li, and C.-Y. Su, "Adaptive neural network control for robotic manipulators with unknown deadzone," *IEEE Trans. Cybern.*, vol. 48, no. 9, pp. 2670–2682, Sep. 2018.

[28] X. Wu, Z. Li, Z. Kan, and H. Gao, "Reference trajectory reshaping optimization and control of robotic exoskeletons for human–robot co-manipulation," *IEEE Trans. Cybern.*, vol. 50, no. 8, pp. 3740–3751, Aug. 2020.

[29] M. Deng, Z. Li, Y. Kang, C. L. P. Chen, and X. Chu, "A learning-based hierarchical control scheme for an exoskeleton robot in human-robot cooperative manipulation," *IEEE Trans. Cybern.*, vol. 50, no. 1, pp. 112–125, Jan. 2020.

[30] J. Li, Z. Li, X. Li, Y. Feng, Y. Hu, and B. Xu, "Skill learning strategy based on dynamic motion primitives for human-robot cooperative manipulation," *IEEE Trans. Cogn. Devel. Syst.*, vol. 13, no. 1, pp. 105–117, Mar. 2021, doi: 10.1109/TCDS.2020.3021762.

[31] L. Kong, W. He, C. Yang, Z. Li, and C. Sun, "Adaptive fuzzy control for coordinated multiple robots with constraint using impedance learning," *IEEE Trans. Cybern.*, vol. 49, no. 8, pp. 3052–3063, Aug. 2019.
[32] L. P. Ureche and A. Billard, "Constraints extraction from asymmetrical bimanual tasks and their use in coordinated behavior," *Robot. Auton. Syst.*, vol. 103, pp. 222–235, May 2018.
[33] R. Caccavale, M. Saveriano, A. Finzi, and D. Lee, "Kinesthetic teaching and attentional supervision of structured tasks in human-robot interaction," *Auton. Robots*, vol. 43, no. 6, pp. 1291–1307, 2019.
[34] B. Nemec, N. Likar, A. Gams, and A. Ude, "Human robot cooperation with compliance adaptation along the motion trajectory," *Auton. Robots*, vol. 42, no. 5, pp. 1023–1035, 2018.
[35] P. Beyl *et al.*, "Safe and compliant guidance by a powered knee exoskeleton for robot-assisted rehabilitation of gait," *Adv. Robot.*, vol. 25, no. 5, pp. 513–535, 2011.
[36] Y. Li, K. P. Tee, W. L. Chan, R. Yan, Y. Chua, and D. K. Limbu, "Continuous role adaptation for human–robot shared control," *IEEE Trans. Robot.*, vol. 31, no. 3, pp. 672–681, Jun. 2015.
[37] D. P. Losey and M. K. O'Malley, "Trajectory deformations from physical human-robot interaction," *IEEE Trans. Robot.*, vol. 34, no. 1, pp. 126–138, Feb. 2018.
[38] X. Yin and L. Pan, "Direct adaptive robust tracking control for 6 DOF industrial robot with enhanced accuracy," *ISA Trans.*, vol. 72, pp. 178–184, Jan. 2018.
[39] X. Yin and L. Pan, "Enhancing trajectory tracking accuracy for industrial robot with robust adaptive control," *Robot. Comput. Integr. Manuf.*, vol. 51, pp. 97–102, Jun. 2018.
[40] L. Pan, G. Bao, F. Xu, and L. Zhang, "Adaptive robust sliding mode trajectory tracking control for 6 degree-of-freedom industrial assembly robot with disturbances," *Assembly Autom.*, vol. 38, no. 3, pp. 259–267, 2018.
[41] L. Pan, T. Gao, F. Xu, and L. Zhang, "Enhanced robust motion tracking control for 6 degree-of-freedom industrial assembly robot with disturbance adaption," *Int. J. Control Autom. Syst.*, vol. 16, no. 2, pp. 921–928, 2018.
[42] X. Gong, T. Zhang, C. L. P. Chen, and Z. Liu, "Research review for broad learning system: Algorithms, theory, and applications," *IEEE Trans. Cybern.*, early access, Mar. 17, 2021, doi: 10.1109/TCYB.2021.3061094.
[43] T. Zhang, Y. Li, and C. L. P. Chen, "Edge computing and its role in Industrial Internet: Methodologies, applications, and future directions," *Inf. Sci.*, vol. 557, no. 3, pp. 34–65, 2021.
[44] T. Zhang, C. Lei, Z. Zhang, X.-B. Meng, and C. L. P. Chen, "AS-NAS: Adaptive scalable neural architecture search with reinforced evolutionary algorithm for deep learning," *IEEE Trans. Evol. Comput.*, early access, Feb. 23, 2021, doi: 10.1109/TEVC.2021.3061466.

Zhijun Li (Senior Member, IEEE) received the Ph.D. degree in mechatronics from the Shanghai Jiao Tong University, Shanghai, China, in 2002.

From 2003 to 2005, he was a Postdoctoral Fellow with the Department of Mechanical Engineering and Intelligent Systems, The University of Electro-Communications, Tokyo, Japan. From 2005 to 2006, he was a Research Fellow with the Department of Electrical and Computer Engineering, National University of Singapore, Singapore, and Nanyang Technological University, Singapore. Since 2017, he has been a Professor with the Department of Automation, University of Science and Technology, Hefei, China, where he was the Vice Dean of the School of Information Science and Technology in 2019. His current research interests include wearable robotics, teleoperation systems, nonlinear control, and neural-network optimization.

Prof. Li has been the Co-Chair of IEEE SMC Technical Committee on Bio-Mechatronics and Bio-Robotics Systems (B^2S) in 2016, and IEEE-RAS Technical Committee on Neuro-Robotics Systems. He is serving as an Editor-at-Large for *Journal of Intelligent & Robotic Systems*, and an Associate Editor for several IEEE TRANSACTIONS.

Guoxin Li received the B.S. degree in mechanical engineering and automation from the Hefei University of Technology, Hefei, Anhui, China, in 2016. He is currently pursuing the Ph.D. degree in automation with the University of Science and Technology of China, Hefei.

His current research interests include human–robot interaction, motion planning and control, and robotic systems.

Xiaoyu Wu received the B.S. degree in automation from Southwest University, Chongqing, China, in 2017, and the M.S. degree in control engineering from the University of Science and Technology of China, Hefei, China, in 2020. She is currently pursuing the Ph.D. degree in biomedical engineering with the National University of Singapore, Singapore.

Her current research interests include human–robot interaction, motion control design, and exoskeleton robotics.

Zhen Kan (Member, IEEE) received the Ph.D. degree from the Department of Mechanical and Aerospace Engineering, University of Florida, Gainesville, FL, USA, in 2011.

He was a Postdoctoral Research Fellow with the Air Force Research Laboratory, Eglin AFB, FL, USA, and the University of Florida Research and Engineering Education Facility, Shalimar, FL, USA, from 2012 to 2016, and was an Assistant Professor with the Department of Mechanical Engineering, University of Iowa, Iowa City, IA, USA, from 2016 to 2019. He is currently a Professor with the Department of Automation, University of Science and Technology of China, Hefei, China. His research interests include networked control systems, nonlinear control, formal methods, and robotics.

Prof. Kan currently serves on program committees of several internationally recognized scientific and engineering conferences and is an Associate Editor for IEEE TRANSACTIONS ON AUTOMATIC CONTROL.

Hang Su (Member, IEEE) received the M.Sc. degree in control theory and control engineering from the South China University of Technology, Guangzhou, China, in 2015, and the Ph.D. degree from the Medical and Robotic Surgery Group, Politecnico di Milano, Milan, Italy, in 2019.

He participated in the EU funded H2020 project (SMARTsurg) in the field of Surgical Robotics. He is currently a Research Fellow with the Department of Electronics, Information and Bioengineering, Politecnico Di Milano. He is fostering an international research team constituting three Ph.D. students and a few master's students in the field of medical robotics.

Dr. Su has served as a reviewer for over 30 scientific journals, such as IEEE TRANSACTION ON BIOMEDICAL ENGINEERING, IEEE/ASME TRANSACTIONS ON MECHATRONICS, IEEE TRANSACTION ON AUTOMATION AND ENGINEERING, IEEE TRANSACTION ON CYBERNETICS, and IEEE TRANSACTIONS ON SYSTEMS, MAN, AND CYBERNETICS: SYSTEMS. He is currently the Special Session Chair of IEEE International Conference on Advanced Robotics and Mechatronics in 2020. He was a member of the Politecnico di Milano in 2019.

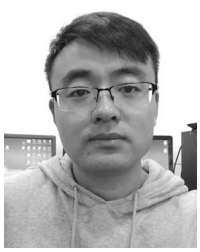

Yueyue Liu received the M.S. and Ph.D. degrees in control engineering from the South China University of Technology, Guangzhou, China, in 2017 and 2021, respectively.

His research interests include bioinspired manipulation and autonomous robot.